Supporting Information

Efficient Non-fullerene Organic Solar Cells Employing Sequentially Deposited Donor-Acceptor Layers

Jiangbin Zhang[1,2#], Bin Kan[3#], Andrew J. Pearson[1], Andrew J. Parnell[4], Joshaniel F.K. Cooper[5], Xiao-Ke Liu[1,6], Patrick J. Conaghan[1], Thomas R. Hopper[2], Yutian Wu[1], Xiangjian Wan[3], Feng Gao[6], Neil C. Greenham[1], Artem A. Bakulin[2], Yongsheng Chen[3], Richard H. Friend[1*]*

[1] Cavendish Laboratory, University of Cambridge, JJ Thomson Avenue, Cambridge CB3 0HE, United Kingdom;

[2] Department of Chemistry, Imperial College London, London SW7 2AZ, United Kingdom;

[3] The Centre of Nanoscale Science and Technology and Key Laboratory of Functional Polymer Materials, State Key Laboratory and Institute of Elemento-Organic Chemistry, College of Chemistry, Nankai University, Tianjin, 300071, China;

[4] Department of Physics & Astronomy, The University of Sheffield, Hicks Building, Hounsfield Road, Sheffield S3 7RH, United Kingdom;

[5] ISIS Neutron and Muon Source, Science and Technology Facilities Council, Rutherford Appleton Laboratory, Didcot, OX11 0QX, United Kingdom;

[6] Department of Physics, Chemistry and Biology (IFM), Linköping University, Linköping SE-58183, Sweden.

[*] yschen99@nankai.edu.cn; rhf10@cam.ac.uk;

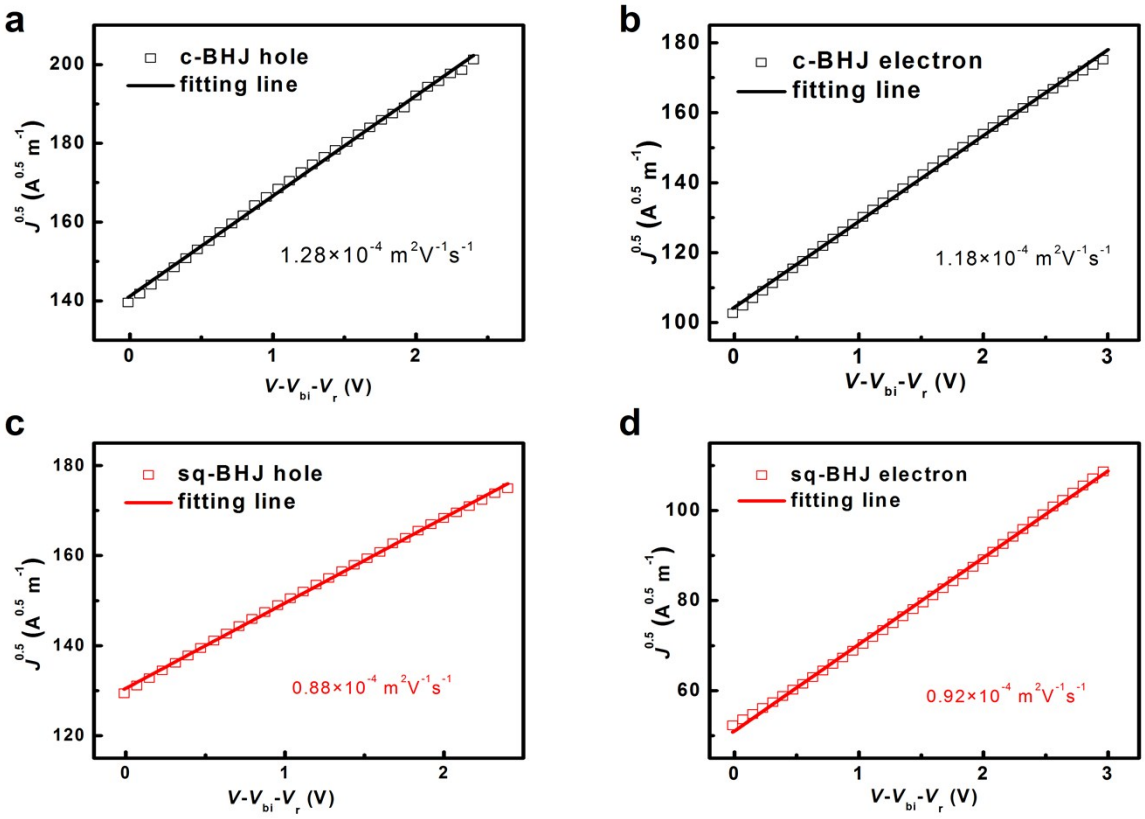

Figure S1. Hole and electron mobilities extracted from the SCLC.

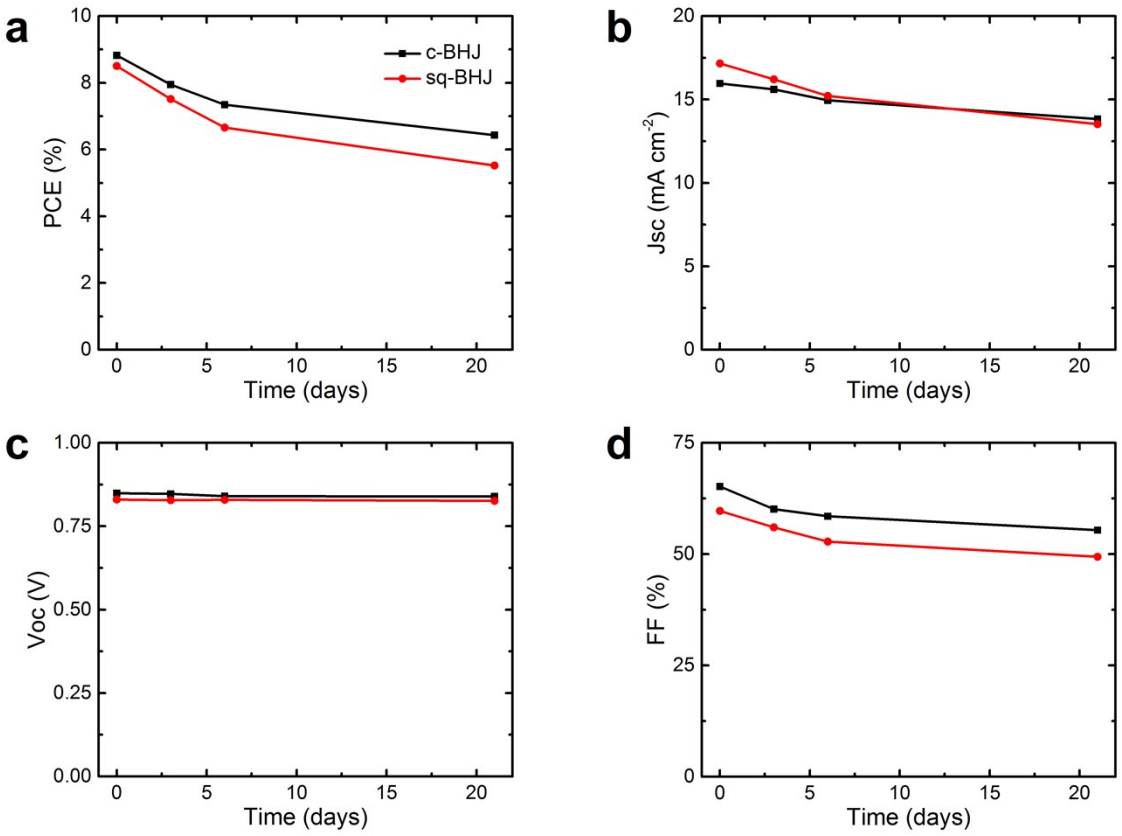

Figure S2. Device stability of c-BHJ and sq-BHJ devices over 3 weeks. The data is averaged of 3 devices. Full dataset is shown in **Table S4**.

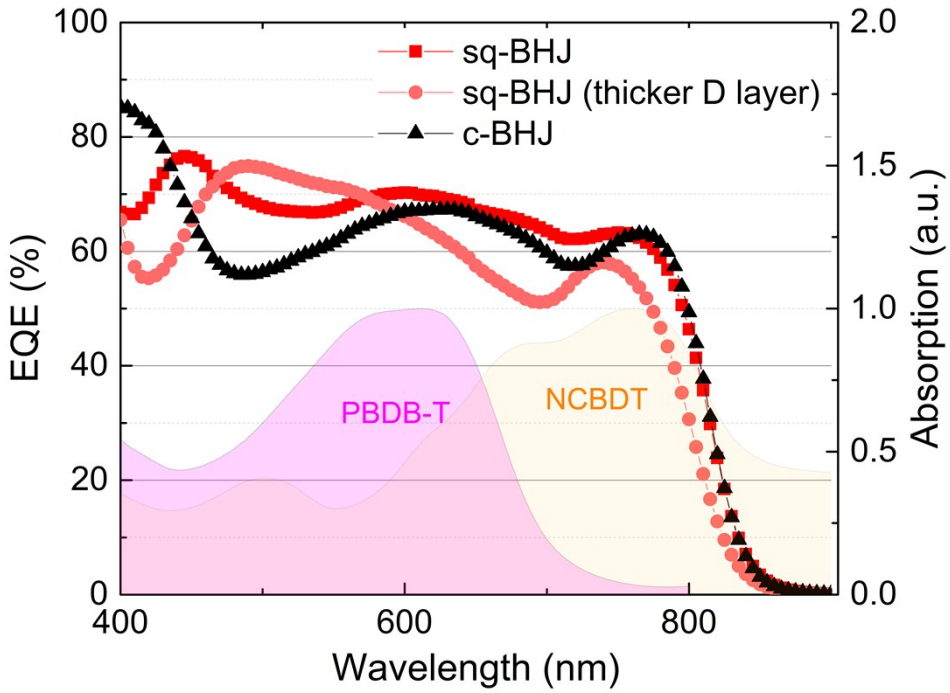

Figure S3. EQE profile of the c-BHJ, and the sq-BHJ devices with different thicknesses of the PBDB-T layer. The filled area shows the absorption profile of PBDB-T and NCBDT.

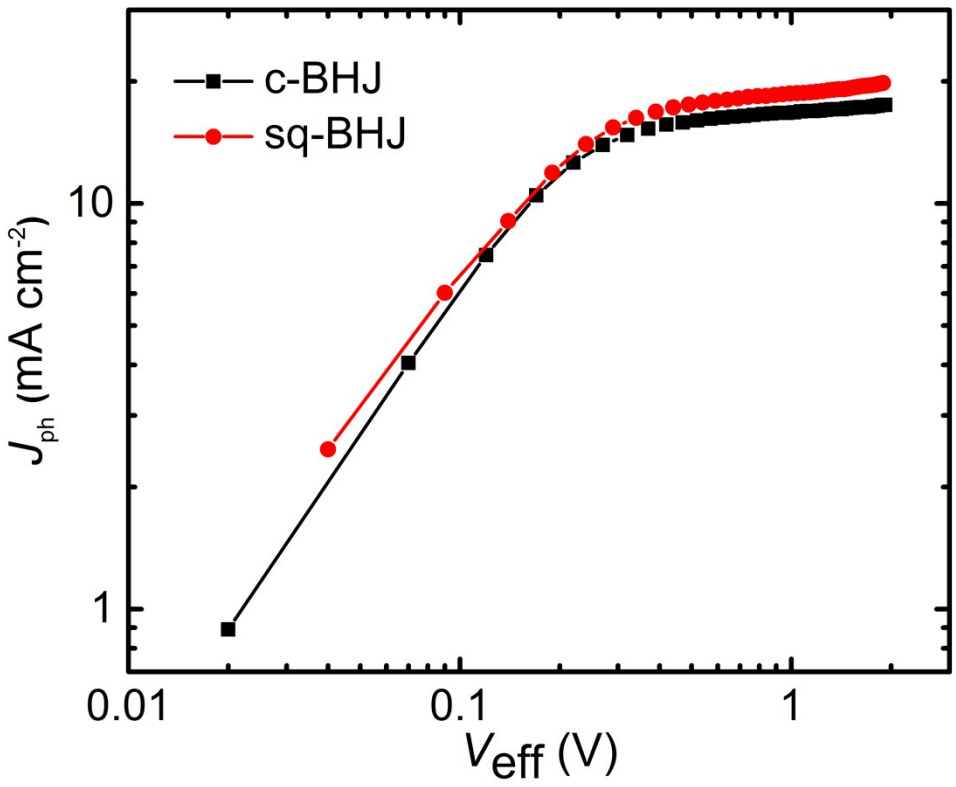

Figure S4. Photocurrent generation versus the effective voltage of c-BHJ and sq-BHJ devices.

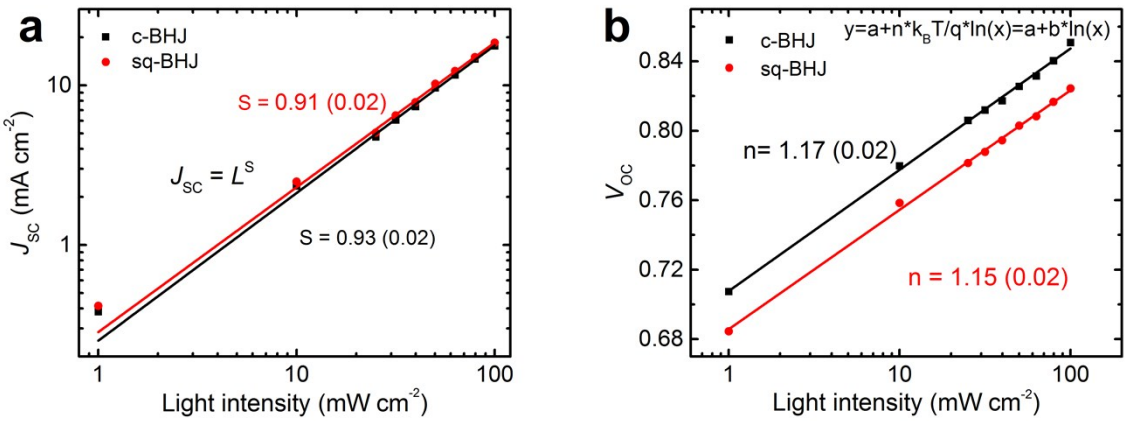

Figure S5. Light-intensity dependent J_{SC} and $V_{OC.}$ The dependence of J_{SC} under different light illumination was fitted as $J_{SC} \propto L^S$, where L is the light intensity, S is the fit parameter. The dependence of V_{OC} on light intensity was fitted with $V_{OC} = a + n * \frac{k_B T}{q} \ln(L) = a + b * ln(L)$, where the slope b is linked to idealty factor n, k_B is the Boltzmann constant, T is the temperature and q is the element charge.

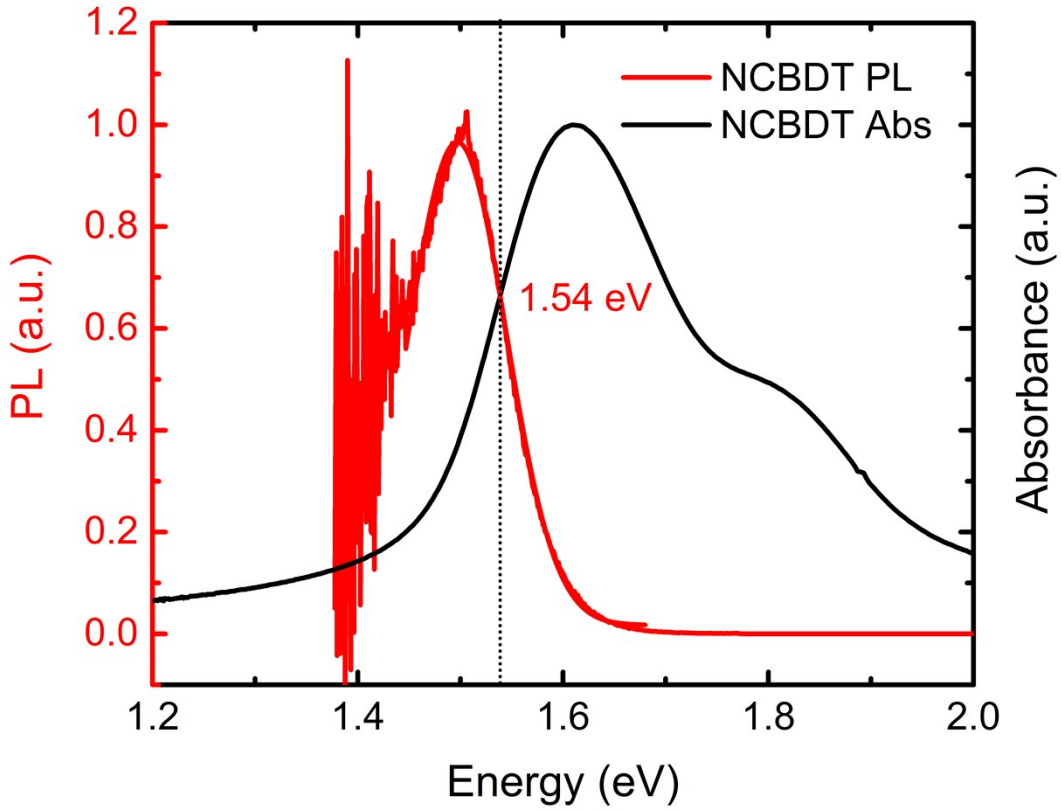

Figure S6. Optical bandgap energy of NCBDT acceptor determined by the cross point of the absorption (black) and emission (red) spectra.

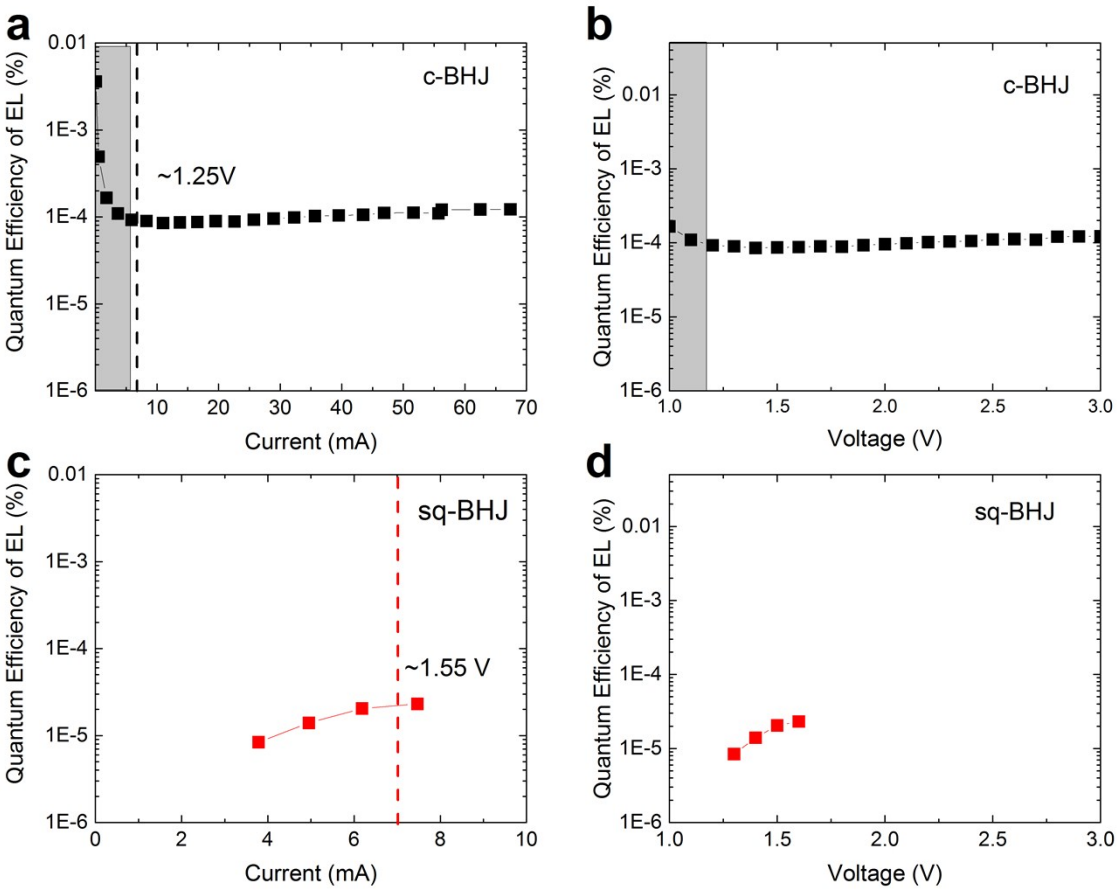

Figure S7. Quantum efficiency of EL of the c-BHJ and sq-BHJ devices. The data in gray region in (a) and (b) is abandoned due to its low luminescence. The EQE_{EL} is determined at the injection current of 7 mA.

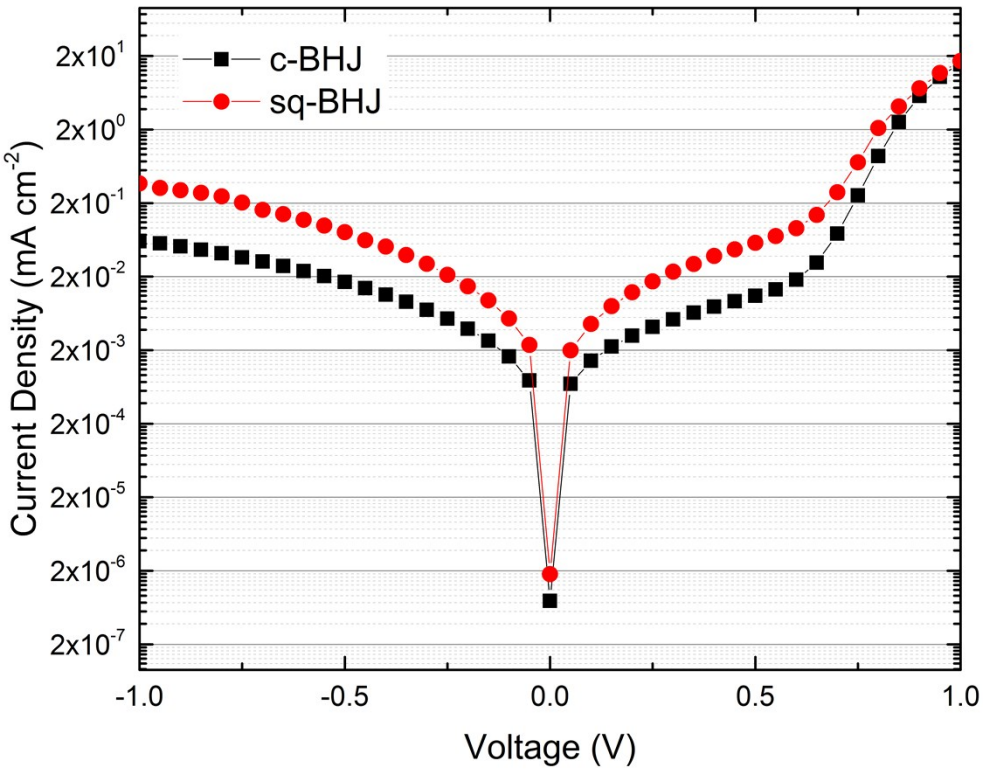

Figure S8. Dark current-density voltage curves of the c-BHJ and sq-BHJ devices.

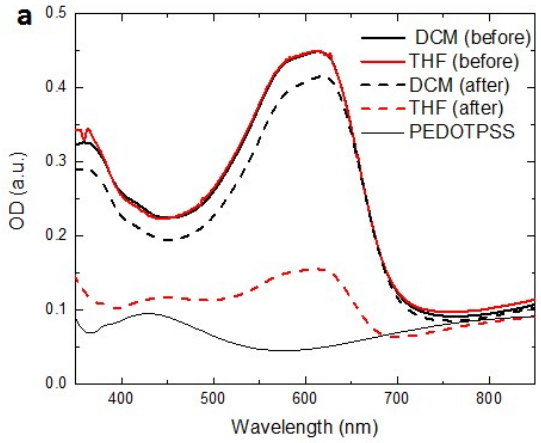

b

c

Sample	Thickness* (nm)	Ra (nm)
Pure PBDB-T	90	0.9
DCM Wash	85	1.7
THF Wash	50	2.0

Figure S9. (a) Films absorption before and after washing the pure PBDB-T layer with THF and DCM. (b) The images of the films after washing. (c) The film thickness (including PEDOT:PSS layer, ~30 nm) and surface roughness measured by AFM.

To initially show the effect of the solvent washing on PBDB-T film, we spin-coated the pristine donor layer with pure THF and DCM, and measured its absorption change as well as its surface roughness. DCM slightly removed the donor layer (5 nm less in thickness and 4% less in absorption) with a smooth surface (Ra = 1.7), while THF largely dissolved the donor layer (40 nm less in thickness and 30% less absorption) with a rougher surface (Ra = 2.0).

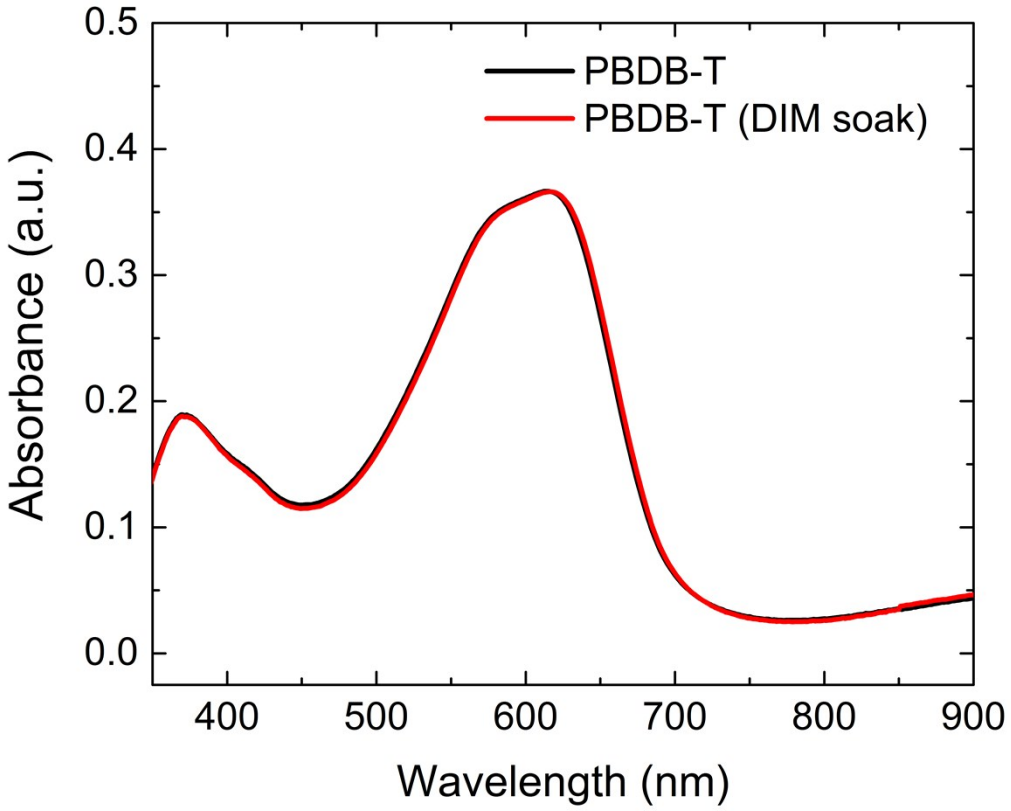

Figure S10. Absorption of PBDB-T film with and without DIM soaking.

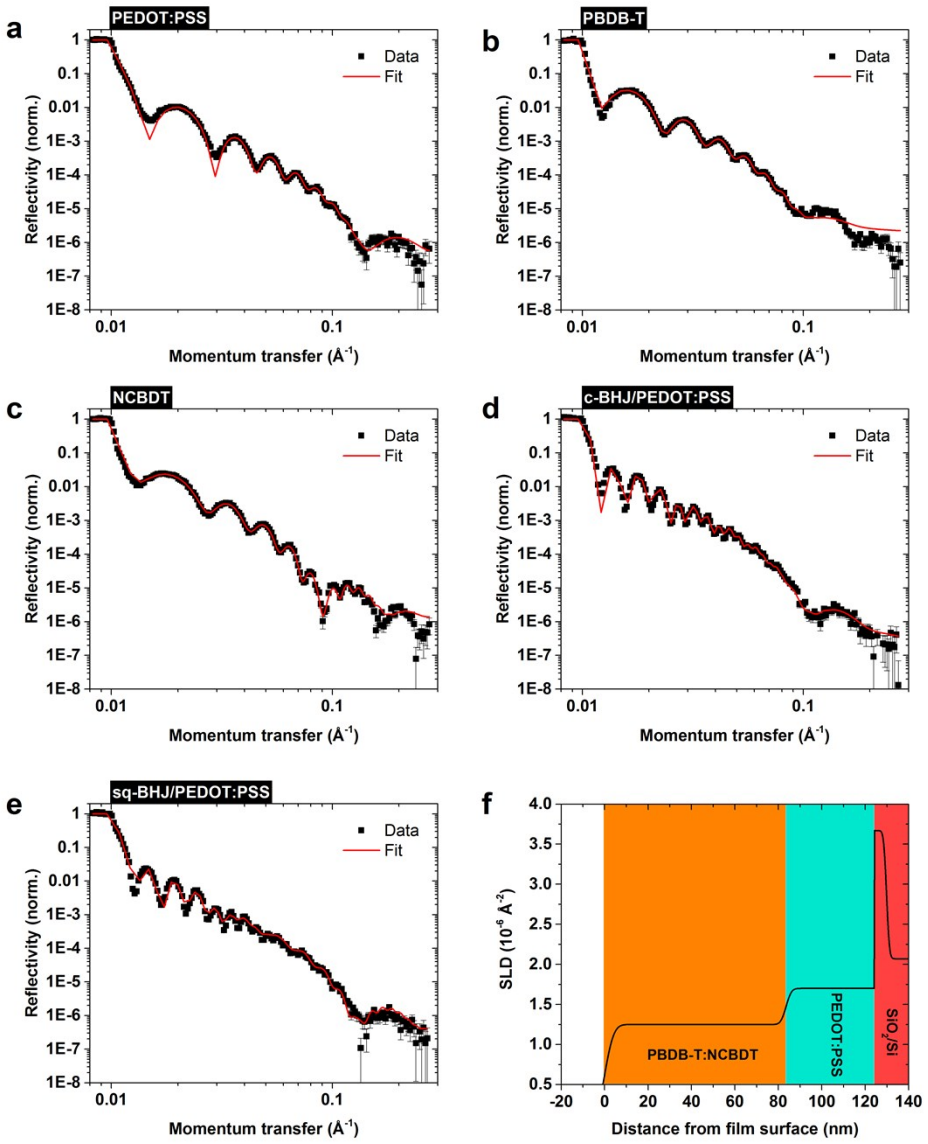

Figure S11. Neutron reflectivity curves of: (a) PEDOT:PSS; (b) PBDB-T; (c) NCBDT; (d) c-BHJ/PEDOT:PSS and (e) sq-BHJ layer/PEDOT:PSS. Each sample was deposited onto a Si substrate with a native oxide layer. The best-fit profile of the scattering length density for the sq-BHJ sample is plotted in (f).

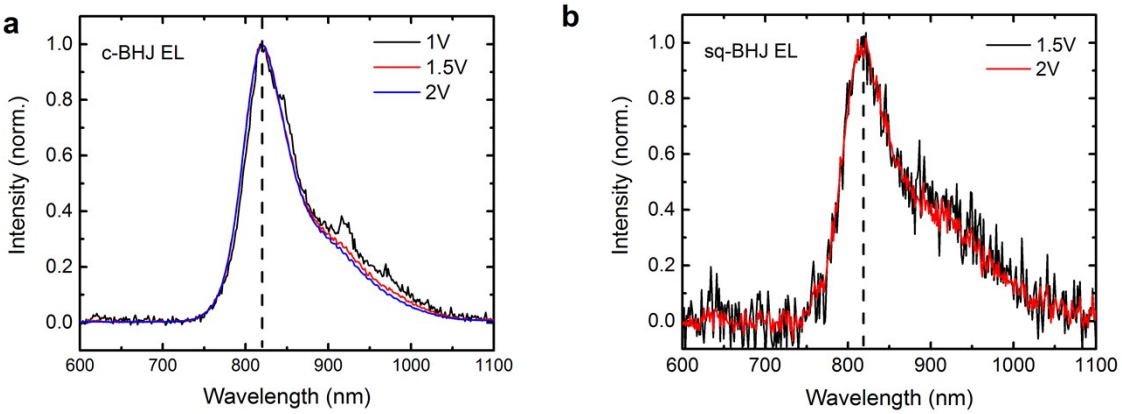

Figure S12. Field-dependent EL of c-BHJ and sq-BHJ devices under forward biases.

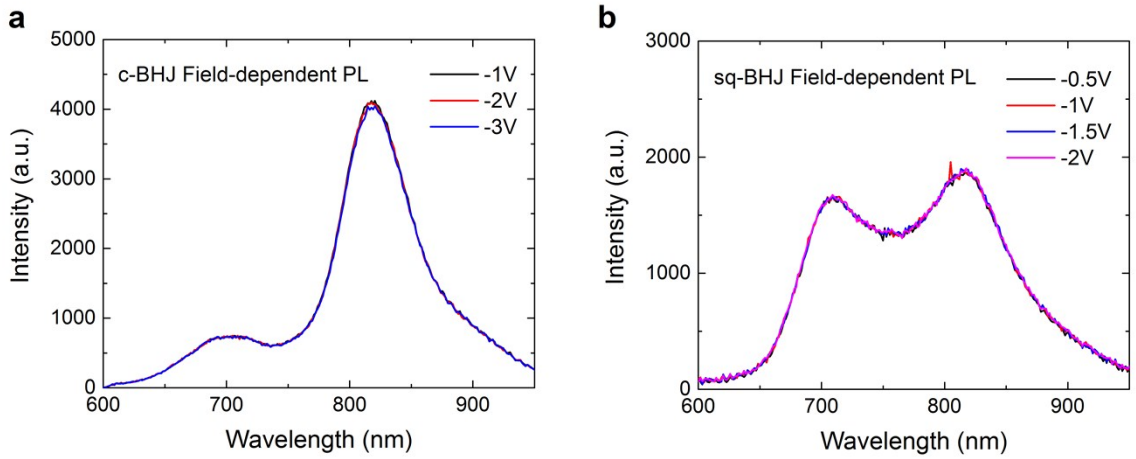

Figure S13. Field-dependent PL of c-BHJ and sq-PHJ OSCs with excitation at 400 nm. The peak at 700 nm is from the emission of PDINO layer. The peak at ~820 nm is from the active layer.

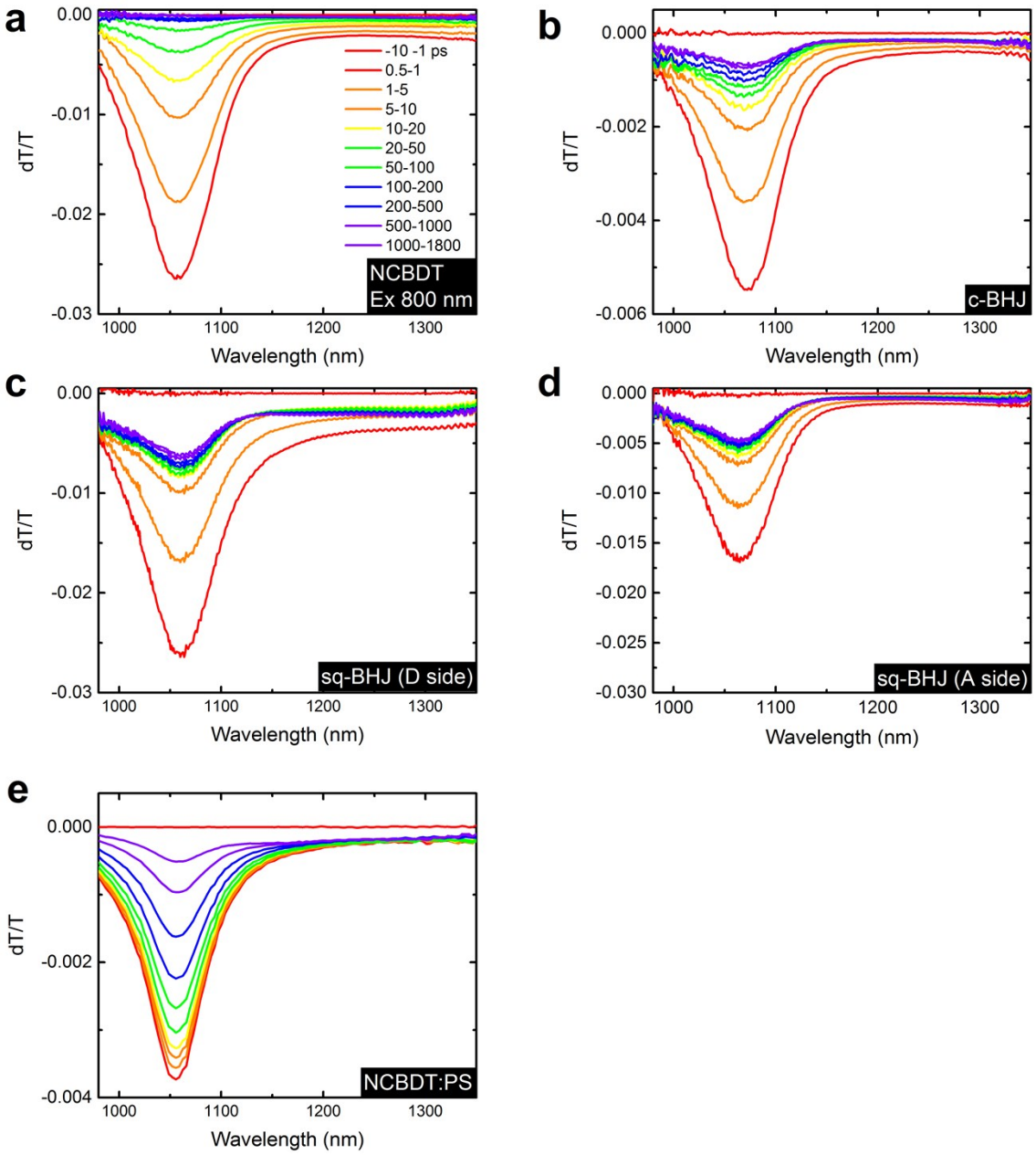

Figure S14. Transient absorption spectra with excitation at 800 nm. (a) pure NCBDT film. (b) c-BHJ film. (c) sq-BHJ film excited with donor side first. (d) sq-BHJ film excited with acceptor side first. (e) NCBDT:PS blend.

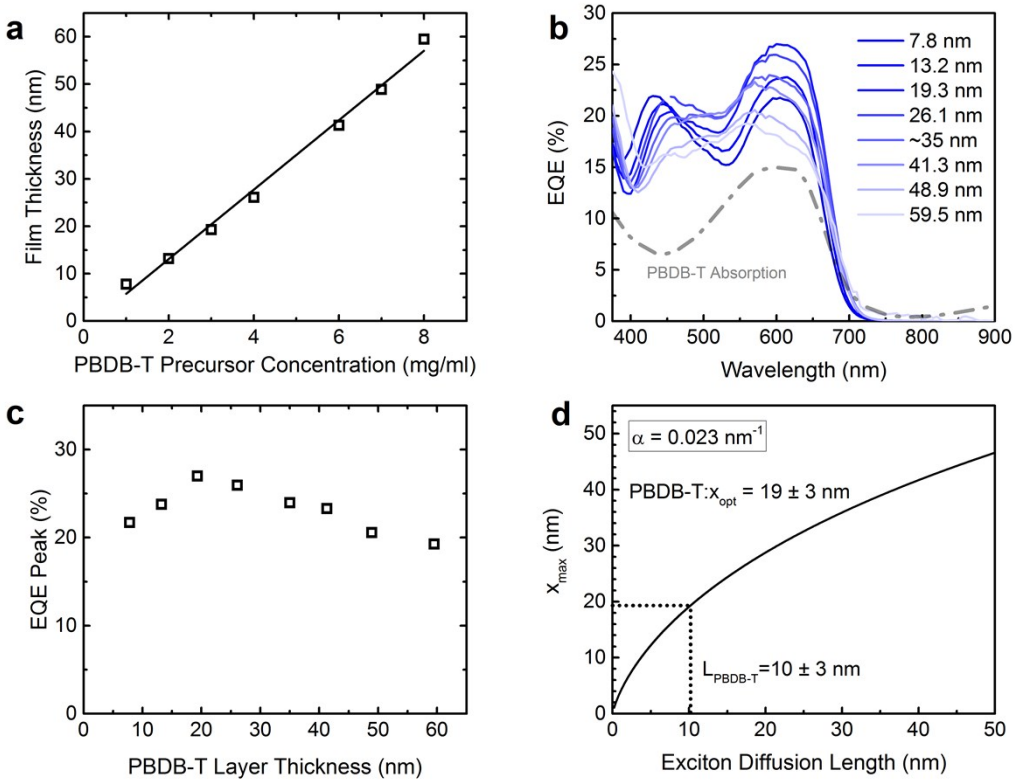

Figure S15. Measurements on exciton diffusion length of PBDB-T. (a) Film thickness of PBDB-T layer deposited from various precursor concentrations (1 mg/ml to 8 mg/ml). (b) EQE spectra of PBDB-T:PCBM PHJ devices. Gray line is the absorption spectrum of PBDB-T. (c) Peak EQE as a function of thicknesses of the PBDB-T layer. (d) Exciton diffusion length (10±3 nm) determined from the optimum donor layer thickness (19±3 nm). The absorption coefficient of PBDB-T film is 2.3×10^5 cm^{-1}.

Table S1. Device optimisation of sq-BHJ devices by varying the solvent for the acceptor layer.

Solvent	V_{OC} (V)	J_{SC} (mA cm^{-2})	FF (%)	PCE (%)
DCM	0.803	19.24	53.8	8.32
DCE	0.811	5.08	43.6	1.79
TCE	0.811	10.15	53.0	4.37

Table S2. Device optimisation by changing the spin speed for the acceptor layer. Donor and acceptor concentration is 6 mg/ml. The spin rate for the donor is 1500 RPM.

Spin speed (RPM)	V_{OC} (V)	J_{SC} (mA cm^{-2})	FF (%)	PCE (%)
1500	0.790	18.80	52.7	7.82
2000	0.799	19.29	53.2	8.19
2500	0.804	19.64	56.7	8.95
3000	0.803	19.24	53.8	8.32
3000+SVA*	0.792	19.57	53.6	8.30

*Solvent vapour annealing treatment after spin-coating the active layer.

Table S3. Device optimisation by changing the spin speed for the donor layer. Donor and acceptor concentration is 6 mg/ml. The spin rate for the acceptor layer is 2500 RPM.

Spin speed (RPM)	V_{OC} (V)	J_{SC} (mA cm^{-2})	FF (%)	PCE (%)
1500	0.804	19.64	56.7	8.95
1700	0.824	19.05	61.7	9.68
1900	0.824	19.45	62.9	10.04
2100	0.791	18.08	58.9	8.42
2300	0.791	18.06	59.2	8.51
1900*	0.803	18.92	59.9	9.10

* The electron transport layer PDINO is replaced with ZnO.

Table S4. Device stability dataset for c-BHJ and sq-BHJ devices.

Device type	Device ID	Day	Voc (V)	FF	Jsc (mA cm^{-2})	PCE (%)
c-BHJ	1	0	0.850	0.653	15.82	8.78
	2	0	0.848	0.647	15.94	8.74
	3	0	0.848	0.655	16.12	8.95
	1	3	0.846	0.605	15.44	7.90
	2	3	0.847	0.594	15.74	7.92
	3	3	0.849	0.603	15.66	8.02
	1	6	0.841	0.580	14.75	7.20
	2	6	0.839	0.582	15.06	7.36
	3	6	0.839	0.592	15.04	7.47
	1	21	0.837	0.557	13.56	6.33
	2	21	0.838	0.557	14.03	6.54
	3	21	0.842	0.549	13.91	6.43
Sq-BHJ	1	0	0.829	0.595	17.17	8.47
	2	0	0.829	0.607	17.15	8.63
	3	0	0.832	0.589	17.16	8.41
	1	3	0.826	0.563	16.28	7.57
	2	3	0.830	0.562	16.04	7.49
	3	3	0.828	0.555	16.32	7.49
	1	6	0.831	0.535	14.95	6.65
	2	6	0.830	0.525	15.21	6.63
	3	6	0.826	0.524	15.46	6.69
	1	21	0.830	0.500	13.33	5.53
	2	21	0.825	0.501	13.42	5.55
	3	21	0.822	0.482	13.82	5.48